Agrociencia

GEOSTATISTICAL ANALYSIS OF THE PHYSICAL PROPERTIES OF GLEYSOL SOIL IN TABASCO, MEXICO

Manuel David **Sosa-García**[1], Maximiano Antonio **Estrada-Botello**[1*], Rufo **Sánchez-Hernández**[1], Carlos Alberto **Pérez-Cabrera**[2], Areli **Carrera-Lanestosa**[1], Pedro **García- Alamilla**[1]

[1]Universidad Juárez Autónoma de Tabasco. Carretera Villahermosa-Teapa km 25, Ranchería La Huasteca 2da. Sección, Villahermosa, Tabasco, Mexico. C. P. 86298.
[2]Colegio Superior Agropecuario del Estado de Guerrero. Avenida Vicente Guerrero 81, Colonia Centro, Iguala de la Independencia, Guerrero, Mexico. C. P. 40000.
* Author for correspondence: maximiano.estrada@ujat.mx

Citation: Sosa-García MD, Estrada-Botello MA, Sánchez-Hernández R, Pérez-Cabrera CA, Carrera-Lanestosa A, García-Alamilla P. 2026. Geostatistical analysis of the physical properties of Gleysol soil in Tabasco, Mexico. **Agrociencia.** https://doi.org/ 10.47163/agrociencia.v60i2.3406

Editor in Chief:
Dr. Fernando C. Gómez Merino

Received: June 17, 2025.
Approved: March 05, 2026.
Published in Agrociencia: March 23, 2026.

ABSTRACT

The water content stored in soil depends on its physical properties and spatial variation. Unfortunately, in the Sierra de Tabasco region, no studies provide information on the spatial variability of water in the soil. Therefore, the objective of this study was to apply geographic information systems to the physical variables of the soil and the water table stored in Gleysol soil on the "La Victoria" farm, in the municipality of Teapa, Tabasco. The physical properties of texture, bulk density (Da), field capacity humidity content (FC), permanent wilting point (PWP), and saturation point (Psat) of the soil were evaluated. The water tables stored at depths of 0–30, 30–60, and 60–90 cm were also assessed. A descriptive statistical analysis was performed, and maps and semivariograms were produced. The results showed that at all three depths, there was a higher percentage of clay content and an average Da of 1.14 g cm^{-3}. The soils had high humidity content, which affects the stored water sheets. For soil properties, the models varied at all three depths and had the lowest R^2 values, while for stored water variation, the R^2 values were greater than 0.9. The construction of maps using geographic information systems is an important tool for understanding the spatial distribution of stored water and determining potential areas with water deficits or excesses.

Keywords: water, semivariograms, field capacity, permanent wilting point.

INTRODUCTION

The spatial distribution of soil physical properties affects the uniform distribution of irrigation water applied in agricultural areas. In addition, the humidity retention capacity of soils affects the availability of water for crops and is the basis for the proper management of water resources and the management and scheduling of irrigation water (Núñez-Ramírez *et al*., 2020). The physical characteristics of soils show complex spatial variability for each soil type, which is influenced by the way they are managed agronomically (Pérez-Zapata *et al*., 2024).

To understand the components of horizontal and transverse water distribution, it is necessary to determine physical characteristics such as texture, structure, porosity, bulk density (Lince-Salazar, 2021), permanent wilting point (PWP), field capacity (FC), and saturation point (Sakaki and Smits, 2015) of the soil. Xu *et al*. (2025) suggest that the permanent wilting point indicates when the soil retains water with such high energy that plants cannot access it, leading to partial or total wilting due to water stress. On the other hand, field capacity is a parameter that indicates how much water a soil can retain against the forces of gravity and is determined by factors linked to soil type, such as texture, structure, the type of clay present, the depth of the wet front, initial humidity, and soil management (Sandoval-García *et al*., 2021).

Soil texture is considered the relative proportion of sand, silt, and clay particles (Márquez, 2021) that influences its water storage capacity, as does bulk density. Some studies indicate that geostatistical techniques in the physical and hydrological properties of soil (bulk density, total porosity, soil humidity and humidity retention) exhibit spatial dependence (Han *et al*., 2024); furthermore, the use of Kriging as a tool determines the spatial variability of soil properties (Awal *et al*., 2019). To make efficient use of water, computational models (Suarez-Muñoz *et al*., 2025) are used with the support of geostatistics, where factors are modeled as spatially correlated random variables (Álvarez-Herrera *et al*., 2021), which helps understand the spatial distribution of water storage in the soil. Several important techniques contribute to this understanding, including geographic information systems (Bautista, 2021).

The Sierra de Tabasco region of Mexico lacks studies on the spatial variability of parameters used to determine the amount of water that soil can store. However, it is assumed that the use of geostatistical tools can help to understand the spatial distribution of soil water content. Therefore, the objective of this study was to utilize geographic information systems techniques to analyze the physical variables of the soil and the water table stored in Gleysol at the "La Victoria" farm in Teapa, Tabasco.

MATERIALS AND METHODS

Study area

The research was conducted at the "La Victoria" banana plantation in the municipality of Teapa, in the state of Tabasco (17° 40′ 59.13" N, 92° 57′ 30.79" W to 17° 41′ 56.32" N, 92° 56′ 39.95" W) (Figure 1). The study area covers 168 ha. The soil corresponds to the mollic Gleysol unit (Palma-López *et al*., 2007). The climate is characterized as hot and humid with rainfall throughout the year (INEGI, 2017). The average annual precipitation is 3085.3 mm, with an average maximum temperature of 32.1 °C, a minimum of 21.1 °C, and a monthly average of 26.6 °C (CONAGUA, 2023), considering the period from 1991 to 2020.

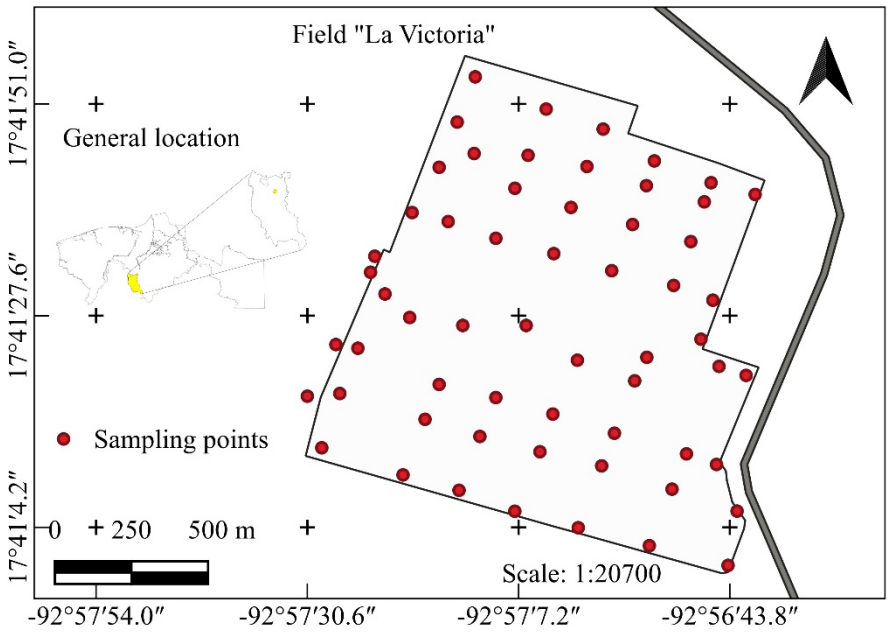

Figure 1. Location of the study area in the municipality of Teapa, Tabasco, Mexico.

Soil sampling

Sampling was carried out during April–May 2023, using a grid system that minimizes the difficulties associated with interpolation, attempting to cover a grid of 180 × 200 m. At some intersections, 55 sampling points were taken, as well as at the periphery of the study area, covering at least one point per 10 ha (Figure 1). Samples were taken at three depths (0–30, 30–60, and 60–90 cm) using an Edelman auger and taken to the Soil and Plant Laboratory of the Academic Division of Agricultural Sciences at the Juárez Autonomous University of Tabasco, where they were dried at room temperature and sieved to determine their physical properties. At the sampling points, the geographical coordinates were determined using a Garmin GPS (GPSMAP 64x) with an accuracy of 3.65 m.

Determination of variables

Texture (Bouyoucos method), bulk density (Da, cylinder method), field capacity (FC, pressure pot method), permanent wilting point (PWP, pressure membrane), and saturation point (Psat, soil saturation) were determined (DOF, 2002). Similarly, the FC sheet, PWP sheet, and Psat sheet were calculated at each of the depths taken.

Calculation of humidity percentage

For the humidity percentage parameters for FC, PWP, and Psat, the wet and dry weights were determined. The humidity percentage was calculated gravimetrically (θw) using the following formula:

$$\theta_w = \frac{(Psh - Pss)}{Pss} * 100$$

where *Psh* is the weight of wet soil (g) and *Pss* is the weight of dry soil (g).

Stored water sheet

The stored leaf area was determined for each stratum using the following formula:

$$Lalmx = \frac{(Px) * Da * Pr}{Dw}$$

where *Lalmx* is the water stored up to the humidity percentage at *FC*, *PWP*, and *Psat* (cm); *Px* corresponds to the gravimetric humidity content (%); *Da* is the bulk density of the soil (g cm^{-3}); *Dw* is the density of water (g cm^{-3}); and *Pr* is the thickness of the soil sheet (cm).

Irrigation sheet

The irrigation sheet was determined for each stratum using the following formula:

$$Lr = \frac{(FC - PWP) * Da * Pr}{Dw}$$

where *Lr* represents the irrigation depth (cm), *FC* the volumetric field capacity (%), *PWP* the volumetric permanent wilting point (%), *Da* the bulk density of the soil (g cm^{-3}), *Dw* the density of water (g cm^{-3}), and *Pr* the thickness of the soil sheet (cm).

Geostatistical analysis

Descriptive statistics were performed using GS+ Version 10 trial software for each of the variables determined. Unmeasured points were estimated using the Kriging method with the following equation:

$$\gamma(h) = \frac{1}{2N(h)} \sum_{i=1}^{n} [Z(X_i) - Z(X_i + h)]^2$$

where $\gamma(h)$ is the semi-variance, $N(h)$ is the number of pairs of points separated by a distance h, $Z(X_i)$ is the heat of the attribute at location Xi, and Z(Xi + h) is the value of the attribute at a distance h from location $X_i + h$.

The best theoretical model was selected according to the structural parameters of the experimental semivariogram: (a) the nugget variance (C_0), which is the Y intercept of the semivariogram model; (b) the sill ($C_0 + C$), which indicates the asymptote of

the curve where the structural variance reaches its maximum values when it remains constant; and (c) the range (A_0), which indicates the distance value (m) at which the maximum soil variance of the parameter is reached, thus defining the area of influence of the autocorrelation (Bautista, 2021).

Map construction

The texture, *FC, PWP*, and *Da* maps were constructed for each stratum, as well as maps of stored water sheets and irrigation in each one. These maps were created using QGIS software and the Kriging interpolation technique. To generate the maps, all variables were classified by range, according to the distribution of cell values resulting from the interpolation.

RESULTS AND DISCUSSION

Descriptive statistics of the soil variables

The statistical parameters (mean, standard deviation, sample variance, maximum and minimum values, skewness, and kurtosis) for the physical properties of the soil (clay, sand, silt, bulk density, field capacity percentage, permanent wilting point percentage, and soil saturation percentage) varied between the depths evaluated (Table 1). For the soil texture components (clay, sand, and silt) in the study area, a minimum percentage of 36.68 % and a maximum of 63.24 % were recorded for clay; for sand, the range was 10.32–36.76 %, while for silt it ranged from 17.44 to 42.01 %. These values correspond to a depth of 60–90 cm.

When comparing the bulk density between depths, the maximum value was found at 60–90 cm and the minimum at 0–30 cm (Table 1). However, in a mollic Gleysol soil in the region, bulk density values of 1.29 to 1.37 g cm^{-3} were reported (Palma-López *et al*., 2007), which are higher than those obtained in this study. The ranges of humidity percentages for *FC, PWP*, and *Psat* were 28.88–46.04, 16.39–29.32, and 53.95–68.78 %, respectively, and varied with depth; in some cases, the values were close to those reported in other studies (Palma-López *et al*., 2007).

The asymmetry values obtained were positive for clay, silt, and permanent wilting point at a depth of 0–30 cm, indicating that the data are distributed to the left of the arithmetic mean. On the other hand, negative asymmetrical values were found in the parameters of sand, bulk density, field capacity, and saturation point, showing that the distribution is skewed to the right in relation to the mean. The kurtosis values were negative in all parameters at a depth of 0–30 cm, indicating a platykurtic distribution. Studies conducted in other locations report asymmetry values of 0.41–0.82 for clay, 0.13–0.46 for sand, and 0.46–0.71 for silt, as well as kurtosis values ranging from -0.55 to 0.43, -0.83 to -0.72, and 0 to 0.33 for clay, sand, and silt, respectively (Varón-Ramírez *et al*., 2022), some of which were similar to those obtained in this study. On the other hand, in a study conducted in Ecuador on Andisol soil, it was found that the kurtosis

Table 1. Descriptive statistics of soil physical properties by depth.

Parameter	Mean	SD	Sample variance	Minimum value	Maximum value	Asymmetry	Kurtosis
				Depth of 0–30 cm			
Clay (%)	46.76	3.90	15.20	40.24	54.52	0.33	-0.80
Sand (%)	26.38	6.18	38.20	11.98	36.76	-0.01	-0.67
Silt (%)	28.98	5.01	25.08	20.72	37.80	0.39	-1.00
Da (g cm^{-3})	1.14	0.05	0.002	1.08	1.22	-0.19	-1.53
FC (%)	37.91	3.46	11.99	30.65	42.87	-0.60	-0.56
PWP (%)	24.01	2.79	7.80	19.02	29.72	0.34	-0.87
Psat (%)	61.74	4.18	17.47	53.95	67.97	-0. 28	-1.31
				Depth of 30–60 cm			
Clay (%)	47.97	6.17	38.13	37.13	60.52	0.21	-0.85
Sand (%)	23.77	5.74	32.95	14.46	36.04	0.16	-0.74
Silt (%)	28.71	5.39	29.02	18.02	30.44	0.24	-0.86
Da (g cm^{-3})	1.13	0.06	0.003	1.04	1.25	0.20	-1.13
FC (%)	39.14	4.01	16.11	31.05	45.99	-0.41	-0.76
PWP (%)	24.14	3.24	10.51	18.80	29.32	0.14	-1.15
Psat (%)	62.19	3.76	14.15	55.00	67.82	-0.33	-1.10
				Depth of 60–90 cm			
Clay (%)	49.41	7.14	51.02	36.68	63.24	0.14	-1.11
Sand (%)	21.75	6.45	41.59	10.32	36.04	0.43	-0.59
Silt (%)	28.41	5.88	36.67	17.44	42.01	0.21	0.59
Da (g cm^{-3})	1.14	0.06	0.06	1.04	1.26	0.17	-1.12
FC (%)	38.79	5.03	25.25	28.88	46.04	-0.37	-0.85
PWP (%)	22.88	3.87	15.00	16.39	29.70	0.06	-1.18
Psat (%)	61.86	3.74	13.98	56.97	68.78	0.19	-1.32

SD: Standard deviation; *Da*: apparent density; *FC*: percentage of humidity at field capacity; *PWP*: percentage of humidity at permanent wilting point; *Psat*: percentage of humidity at saturation point.

and skewness of the bulk density were close to zero at different depths (Salamanca-Jiménez *et al*., 2018), which differs from the results obtained in this study, possibly due to the type of soil.

The results of the descriptive parameters for the depth of 30–60 cm show that all parameters, with the exception of field capacity and saturation, presented positive asymmetry. In terms of kurtosis, all parameters showed negative values, indicating a platykurtic distribution. Likewise, the variables presented differences in asymmetry and kurtosis, without reflecting a clear trend regarding depth.

The descriptive statistical parameters of the water sheets stored in the soil were not similar among the three depths evaluated (Table 2) and varied according to depth. The asymmetry of the variables evaluated was also not similar at the three depths; however, the kurtosis was negative in all variables and depths, indicating platykurtic distributions. On the other hand, the total average water storage was 39.27 cm at field

Table 2. Descriptive statistical parameters of water stored in the soil at different depths.

Parameter	Mean (cm)	SD	Sample variance	Minimum value (cm)	Maximum value (cm)	Asymmetry	Kurtosis
				Depth of 0–30 cm			
Lr_{FC}	12.88	0.68	0.47	11.24	14.31	-0.15	-0.54
Lr_{PWP}	8.24	0.46	0.21	7.26	9.58	0.27	-0.71
Lr_{Psat}	21.33	0.91	0.83	19.23	23.40	-0.12	-0.66
$Lr_{FC\text{-}PWP}$	4.64	0.68	0.46	3.16	6.16	0.53	-0.44
				Depth of 30–60 cm			
Lr_{FC}	13.20	0.57	0.32	11.84	14.39	0.36	-0.54
Lr_{PWP}	8.08	0.54	0.29	6.81	9.51	0.13	-0.41
Lr_{Psat}	20.98	0.64	0.41	19.48	22.60	-0.12	-0.68
$Lr_{FC\text{-}PWP}$	5.12	0.52	0.27	3.58	6.54	0.30	-0.11
				Depth of 60–90 cm			
Lr_{FC}	13.27	0.97	0.94	10.80	15.89	0.06	-0.57
Lr_{PWP}	7.67	0.97	0.95	5.84	10.05	0.17	-0.88
Lr_{Psat}	21.11	0.87	0.75	19.22	23.59	0.25	-0.74
$Lr_{FC\text{-}PWP}$	5.60	0.82	0.66	2.83	7.40	-0.28	-0.50

SD: Standard deviation; Lr_{FC}: sheet stored up to field capacity; Lr_{PWP}: sheet stored up to permanent wilting point; Lr_{Psat}: sheet stored up to saturation point; $Lr_{FC\text{-}PWP:}$ sheet stored between field capacity and permanent wilting point (replacement sheet).

capacity, 23.99 cm at permanent wilting point, and 63.42 cm at saturation, while the replacement water storage (between *FC* and *PWP* humidity) was 15.36 cm.

Semivariograms

Physical properties of the soil

At a depth of 0–30 cm, the Gaussian model provided the best fit for the parameters clay, sand, and saturation point; the spherical model for silt and field capacity; and the exponential model for permanent wilting point and bulk density. In the parameters evaluated, the nugget percentages ranged from 0.00001 to 21.09 %, with R^2 values from 0.536 to 0.919 (Table 3). The sand and permanent wilting point parameters showed the best fit to the statistical model, while clay had the lowest R^2.

At a depth of 30–60 cm, the semivariograms were adjusted to Gaussian and spherical models, depending on the soil property. R^2 values between 0.5 and 0.931 were recorded, ranges between 212 and 1299 m, and nugget percentages from 0.0001 to 14.18 %. At a depth of 60–90 cm, the semivariograms were adjusted to exponential, spherical, and Gaussian models. R^2 values ranged from 0.55 to 0.99, nugget percentages from 0.00015 to 25.2 %, and ranges were between 271 and 6132 m. The sand parameter recorded the highest nugget percentage and the lowest coefficient of determination.

Table 3. Parameters and adjustment of semivariogram models for soil properties and water depth.

Parameter	Model	Nugget (C_0 %)	Sill ($C_0 + C$)	Range (A_0 m)	Structural variance (%)	R^2
			Depth of 0–30 cm			
Clay	Gaussian	0.10	14.680	216.51	99.90	0.54
Sand	Gaussian	21.09	47.100	1039.23	55.20	0.92
Silt	Spherical	0.01	24.650	195.00	100.00	0.73
Da	Exponential	0.00001	0.00244	1038.00	100.00	0.83
FC	Spherical	0.96	12.220	464.00	92.10	0.81
PWP	Exponential	1.17	9.313	990.00	87.40	0.91
Psat	Gaussian	6.60	43.200	1376.98	84.70	0.87
Lr_{FC}	Gaussian	0.001	0.530	464.18	1.00	0.96
Lr_{PWP}	Gaussian	0.0424	0.270	1364.86	0.85	0.98
Lr_{Psat}	Gaussian	0.063	0.986	566.381	0.94	0.99
$Lr_{FC\text{-}PWP}$	Gaussian	0.079	0.538	777.69	0.85	0.92
			Depth of 30–60 cm			
Clay	Gaussian	3.30	38.080	244.21	91.30	0.88
Sand	Spherical	14.18	40.710	1299.00	65.20	0.91
Silt	Spherical	0.01	29.580	212.00	100.00	0.62
Da	Gaussian	0.0001	0.00421	304.84	99.80	0.76
FC	Spherical	5.38	15.200	447.00	66.80	0.50
PWP	Spherical	2.77	12.380	858.00	77.60	0.90
Psat	Spherical	2.29	26.020	732.00	85.70	0.93
Lr_{FC}	Gaussian	0.012	0.368	464.19	0.97	0.90
Lr_{PWP}	Gaussian	0.005	0.376	748.24	0.99	0.99
Lr_{Psat}	Gaussian	0.058	0.467	642.59	0.88	0.98
$Lr_{FC\text{-}PWP}$	Gaussian	0.0109	0.316	519.62	0.98	0.98
			Depth of 60–90 cm			
Clay	Gaussian	0.10	47.410	259.81	99.80	0.70
Sand	Exponential	25.2	81.400	6132.00	69.00	0.60
Silt	Spherical	0.10	38.430	271.00	99.70	0.74
Da	Spherical	0.0002	0.004	388.00	96.10	0.94
FC	Gaussian	0.54	26.320	462.45	80.00	0.98
PWP	Spherical	0.01	20.330	978.00	100	0.98
Psat	Spherical	5.23	21.130	2110.00	75.20	0.92
Lr_{FC}	Spherical	0.081	1.746	2602.00	0.954	0.99
Lr_{PWP}	Gaussian	0.039	1.196	862.56	0.97	1.00
Lr_{Psat}	Gaussian	0.153	0.933	1066.94	0.84	0.97
$Lr_{FC\text{-}PWP}$	Gaussian	0.139	0.668	762.10	1.00	0.99

Da: bulk density; *FC*: percentage of humidity at field capacity; *PWP*: percentage of humidity at permanent wilting point; *Psat*: percentage of humidity at saturation point; Lr_{FC}: leaf stored up to field capacity; Lr_{PWP}: leaf stored up to permanent wilting point; Lr_{Psat}: leaf stored up to saturation point; $Lr_{FC\text{-}PWP}$: leaf stored between field capacity and permanent wilting point (replacement leaf).

For the apparent density variable, Li *et al*. (2019) report that the best fit model was exponential in the 0–20 cm layer, spherical at depths of 20–40 and 40–60 cm, and Gaussian at a depth of 60–100 cm. In addition, the R^2 values were lower and the nugget percentages were higher than those recorded in this study. Salamanca-Jiménez *et al*. (2018) point out that the spherical model presented the best fit in their research, which is consistent only with the 60–90 cm depth in this study.

Stored water sheets

The semivariograms of the water sheets stored at field capacity, at the point of permanent wilting, and at replacement, at all three depths, were adjusted to the Gaussian model, with R^2 values greater than 0.9. Meanwhile, the sheet stored at field capacity at a depth of 60–90 cm was adjusted to a spherical model.

The nugget effect should not be interpreted as a direct measure of error. It is more accurately defined as a phenomenon that represents the randomness inherent in regionalized variables and their values (Camana and Deutsch, 2019); however, it contributes to determining data quality. Even when the spatial separation between samples is minimal, variability exists, and the discrepancy between samples taken very close together complicates the interpolation process due to the high variability of the parameter. Therefore, the nugget effect can be considered a quantitative measure of the level of variability between samples located at very short distances (Yu *et al*., 2025). Parameters with low nugget percentages have less variability and a more homogeneous and predictable distribution; conversely, high nugget values indicate high randomness and, consequently, less reliable predictions.

The nugget effect describes whether a parameter, when sampled again at the same location, will produce similar results or not (Behrens *et al*., 2019). In this study, the sand variable had the highest nugget percentages at all three depths. The model with the lowest fit corresponded to field capacity at a depth of 30–60 cm; however, this same parameter at a depth of 60–90 cm recorded the highest R^2 value.

Construction of maps

Texture

Clay occupied the largest surface area at all three depths, ranging from 43 to 48 % (Figure 2). Clay was the predominant fraction at all depths, with the largest surface area in the 0–30 cm stratum, which is consistent with the report by SEMARNAT (2024), which classifies the soils in the study area as clayey. CONABIO (2020) classifies the soils in the area as Gleysols, coinciding with Palma-López *et al*. (2007), who identify them as mollic Gleysols. In this type of soil, clay contents of 34.3, 40.1, and 21.4 % were reported at depths of 0–38, 38–70, and 70–99 cm, respectively, values that differ from those obtained in this study and from the sampling depths considered.

According to the clay content predictions proposed by CONABIO (2020), percentages of 24.3–26.48 % were reported in the study area at a depth of 0–5 cm, 24.5–26.83 % at

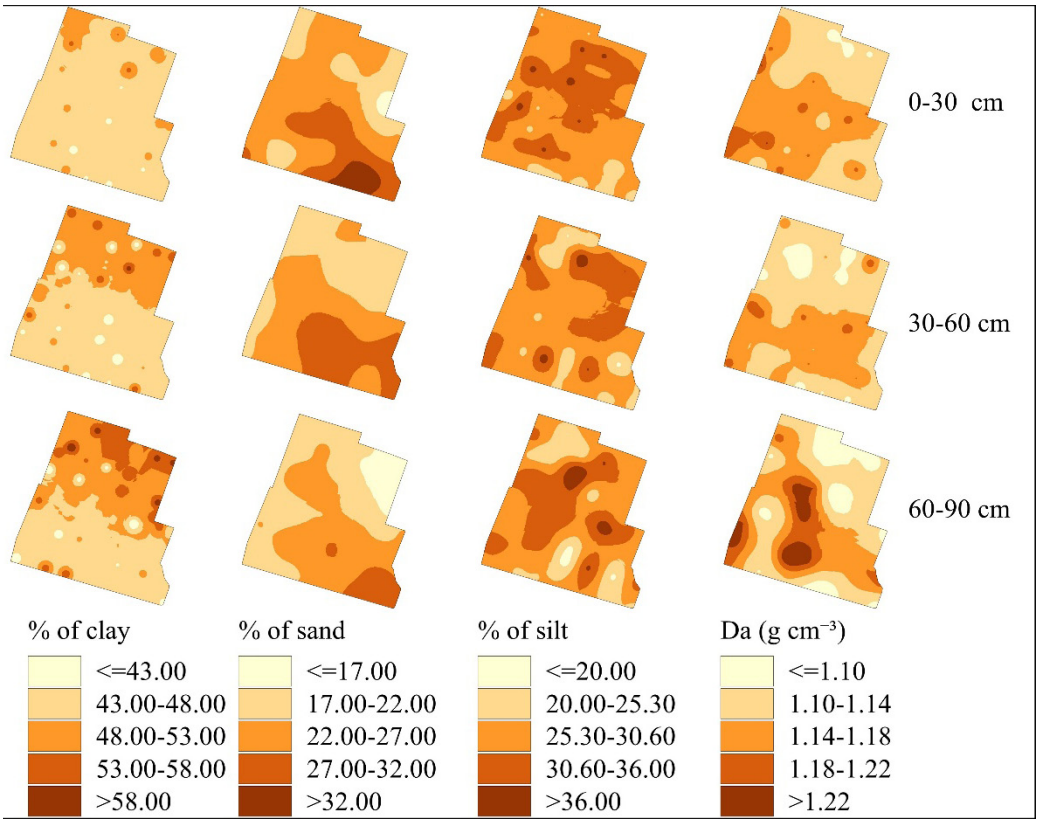

Figure 2. Spatial distribution of soil texture (clay, sand, and silt) and bulk density (*Da*) at the three depths evaluated.

5–15 cm, 28.08–30. 2 % at 15–30 cm, 32.33–33.37 % at 30–60 cm, and 33.9–35.36 % at 60–90 cm, which are lower than those obtained in this research. This difference is due to the fact that these studies are carried out with sampling points established in grids with separations exceeding 1 km between points.

Sand

The sand content at a depth of 0–30 cm was present in more than 50 % of the study area, varying between 22 and 27 %. At a depth of 30–60 cm, this same range occupied the largest surface area (39.78 %), while the rest of the area was distributed between the ranges of 17–22 and 27–32 %, as no values lower than 17 % or higher than 32 % were recorded at this depth. At a depth of 60–90 cm, no values above 32 % were observed; however, more than 80 % of the study area had sand contents between 17 and 27 %. In contrast, CONABIO (2020) reports sand percentages in the study area ranging from 40–56.38, 39.64–41.29, 40.32–40.96, 35.79–36.86, and 34–44.04 % at depths of 0–5, 5–15, 15–30, 30–60, and 60–90 cm, respectively. On the other hand, based on the soil profile corresponding to the soil type, sand percentages of 40.7, 39.3, and 38.75 %

are reported at depths of 0–38, 38–70, and 70–99 cm, respectively (Palma-López *et al*., 2007), which are higher than those found in this research.

Silt

As for the percentage of silt, at all three depths (0–30, 30–60, and 60–90 cm), the class of 25.3–30.6 % predominated, with 57.56, 59.43, and 48.16 % of the total area, respectively. In the study area, 24.6, 20.6, and 39.4 % of silt are reported at depths of 0–38, 38–70, and 70–99 cm, respectively (Palma-López *et al*., 2007), which is close to the data obtained in this research when considering the class with the largest surface area occupied. On the other hand, CONABIO (2020) reports, for the depth of 0–5 cm, percentages of silt in the range of 17.73–33.51 %; from 32.49–34.52 % at 5–15 cm; from 29.30–30.96 % at 15–30 cm; 30–31.60 % at 30–60 cm; and 20.59–32.11 % at 60–90 cm.

Bulk density

The bulk density at a depth of 0–30 cm showed two classes (1.10–1.14 and 1.14–1.18 g cm^{-3}) covering more than 90 % of the area (Figure 2). Similar behavior was observed at depths of 30–60 and 60–90 cm, where these ranges covered 68 % of the surface. These values indicate a variation between the strata evaluated and show that they are not homogeneous, contrary to what has been reported in other studies. This parameter is relevant because of its relationship with other physical and chemical properties of the soil and because it provides information on its use and management, which has a direct effect on plant growth (Salamanca-Jiménez *et al*., 2018).

Percentage of humidity at field capacity

At a depth of 0–30 cm, the highest field capacity values were concentrated in the northern and southeastern parts of the study area (Figure 3); at a depth of 30–60 cm, these values were mainly distributed in the western and southeastern areas; and at a depth of 60–90 cm, the highest values were located in the northern area, which is related to the clay content present. In terms of field capacity percentages, values of 13.91, 16.02, and 8.57 % are reported for depths of 0–38, 38–70, and 70–99 cm, respectively (Palma-López *et al*., 2007), which are lower than those obtained in this study. Conversely, both field capacity and the permanent wilting point increased significantly with sampling depth, aligning with the values reported by Amsili *et al*. (2024).

Percentage of humidity at the point of permanent wilting

In the 0–30 and 30–60 cm strata, the permanent wilting point showed the highest percentage in the range of 21–23.6 % humidity. In contrast, at a depth of 60–90 cm, the highest percentage corresponded to a value of 21 %. In terms of spatial distribution, the lowest PWP values are located in the southern part of the study area (Figure 3), which is associated with a lower apparent density in this zone, a condition that influences PWP, as has been noted in other studies (Chicas-Soto *et al*., 2014).

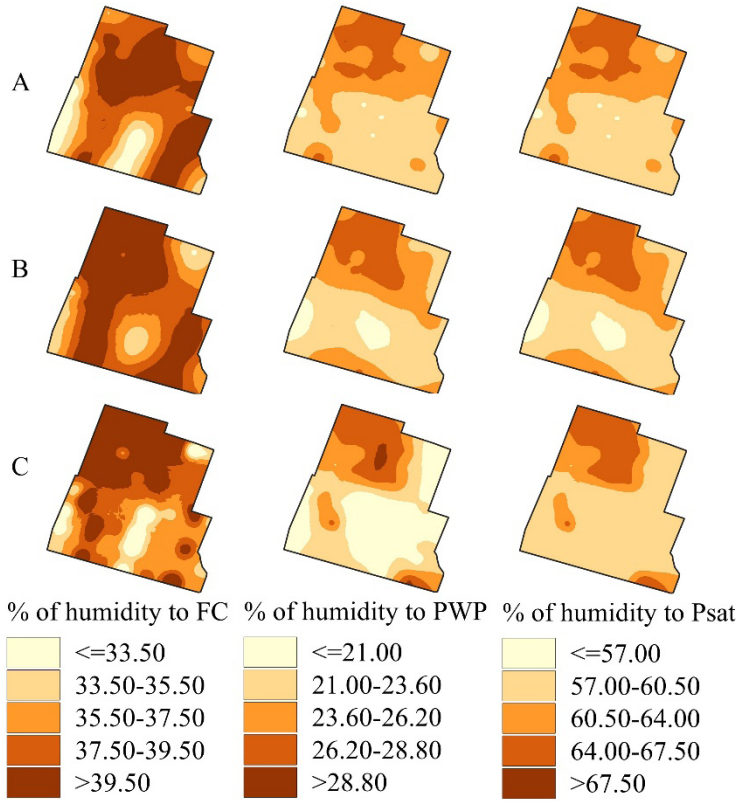

Figure 3. Spatial distribution of the percentage of humidity at field capacity (FC), permanent wilting point (PWP), and saturation point (Psat). A: Depth 0–30 cm; B: depth 30–60 cm; C: depth 60–90 cm.

Percentage of humidity at saturation point

At all three depths, the percentage of humidity saturation ranged between 57 and 67.5 %, which is associated with the high clay content of the soils and directly influences humidity retention (Chicas-Soto *et al*., 2014). Furthermore, as soil bulk density increased, so did the saturation humidity content (Alonso-Báez *et al*., 2023). At depths of 30–60 and 60–90 cm, no areas with saturation humidity content above 67.5 % were recorded. The lowest values of saturation humidity at the three depths were mainly concentrated in the southwest of the study area, while the highest values were associated with the north and northwest, particularly at a depth of 60–90 cm (Figure 3), where the highest clay content was found.

Water sheet stored in the soil

In this study, the replacement sheet was grouped into five classes: ≤12.9, 12.9–14.59, 14.59–16.28, 16.28–17.97, and >17.9 cm; nearly 90 % of the total area has a replacement sheet between 12.9 and 17.97 cm. This result implies the existence of a variable irrigation

rate and the need to avoid problems of water stress in plants, as noted in other studies (Reza *et al*., 2016). The information obtained from the maps allows the modeling of the humidity retention capacity of soils and shows the presence of spatial variation.

The sheet stored in the soil to the point of permanent wilting showed the highest values in the northwestern part of the study area. The humidity content at field capacity showed a distribution very similar to that of the 30–60 cm depth for this same parameter, with the highest values in the western and southeastern parts of the study area. Meanwhile, the humidity content at saturation showed its highest values in the northern part of the study area (Figure 4).

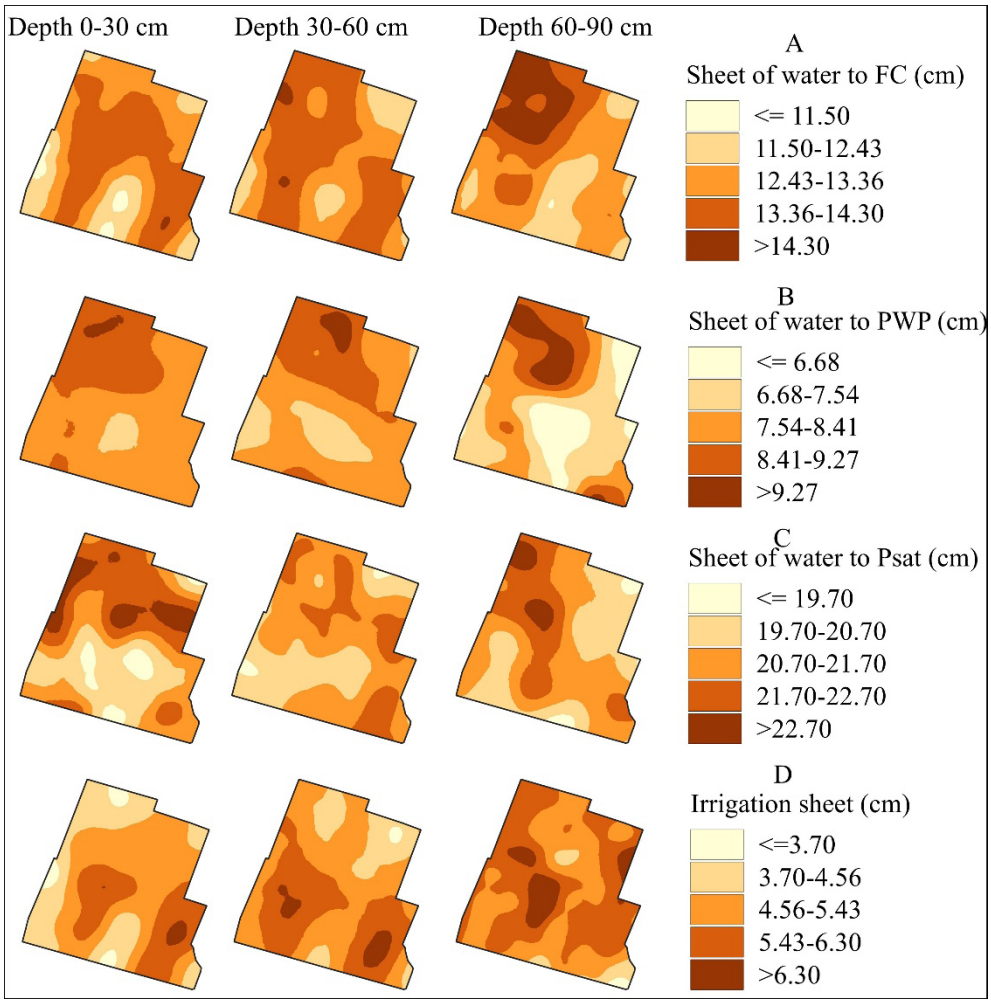

Figure 4. Spatial distribution of stored water depth (in cm). A: field capacity (FC) B: permanent wilting point (PWP) C: saturation point D: depth between CC and PWP (irrigation depth).

CONCLUSIONS

The water storage sheets for the 0–90 cm stratum showed a non-homogeneous spatial distribution in the 168 ha study area of the "La Victoria" farm in Teapa, Tabasco, both for the sheets corresponding to field capacity humidity content, permanent wilting point, saturation humidity, and replacement sheet. The application of geographic information systems made it possible to identify the areas with the greatest water storage potential at different depths. The creation of maps helped to visualize the areas with the highest and lowest amounts of water stored in the farm's soil. In addition, the physical properties of the soil determined the water content stored in the stratum, which was influenced by bulk density, field capacity, permanent wilting point, and saturation point.

ACKNOWLEDGEMENTS

We would like to thank the Juárez Autonomous University of Tabasco for its support in carrying out the project "Water requirements for banana cultivation in a river floodplain area in the municipality of Teapa," code 20221158.

REFERENCES

Alonso-Báez M, López-Guillen G, Grajales-Solís M. 2023. Mejoramiento de las propiedades hidráulicas del suelo en el cultivo de soya mediante el subsuelo. Revista Mexicana de Ciencias Agrícolas 14 (5): 78–89. https://doi.org/10.29312/remexca.v14i5.3102

Álvarez-Herrera JG, Ruiz-Berrío HD, Acosta-Tova DF. 2021. Evaluación geoestadística de atributos hidrofísicos del suelo en la granja Tunguavita, Paipa, Colombia. Ciencia e Ingeniería Neogranadina 31 (1): 127–138. https://doi.org/10.18359/rcin.5396

Amsili JP, van Es HM, Schindelbeck RR. 2024. Pedotransfer functions for field capacity, permanent wilting point, and available water capacity based on Random Forest models for routine soil health analysis. Communications in Soil Science and Plant Analysis 55 (13): 1967–1984. https://doi.org/10.1080/00103624.2024.2336573

Awal R, Safeeq M, Abbas F, Fares S, Deb SK, Ahmad A, Fares A. 2019. Soil physical properties spatial variability under long-term no-tillage corn. Agronomy 9 (11): 750. https://doi.org/10.3390/agronomy9110750

Bautista F. 2021. Geostatistical analysis of soil properties of the karstic sub-horizontal plain of the Yucatan Peninsula. Tropical and Subtropical Agroecosystems 24 (1). https://doi.org/10.56369/tsaes.3540

Behrens T, Viscarra-Rossel RA, Kerry R, MacMillan R, Schmidt K, Lee J, Scholten T, Zhu AX. 2019. The relevant range of scales for multi-scale contextual spatial modelling. Scientific Reports 9 (1). https://doi.org/10.1038/s41598-019-51395-3

Camana FA, Deutsch CV. 2019. The nugget effect. *In* Deutsch JL. (ed.), Geostatistics Lessons. http://geostatisticslessons.com/lessons/nuggeteffect (Retrieved: December 2025)

Chicas-Soto RA, Vanegas-Chacón EA, García-Álvarez N. 2014. Determinación indirecta de la capacidad de retener humedad en suelos de la subcuenca del río Torjá, Chiquimula, Guatemala. Revista Ciencias Técnicas Agropecuarias 23 (1): 41–46.

CONABIO (Comisión Nacional para el Conocimiento y Uso de la Biodiversidad). 2020. Edafología. Mapeo digital de suelos, propiedades del suelo. 1000m. Catálogo de metadatos geográficos. Ciudad de México, México. http://www.conabio.gob.mx/informacion/gis/?vns=gis_root/edafo/edfmdsuelo/edfmscsue/edfmscsu1m/cly_05cm_pgw (Retrieved: December 2025).

CONAGUA (Comisión Nacional del Agua). 2023. Normales climatológicas por estado. Gobierno de México. Comisión Nacional del Agua. Ciudad de México, México. https://smn.conagua.gob.mx/es/climatologia/informacion-climatologica/normales-climatologicas-por-estado?estado=tab (Retrieved: December 2025).

DOF (Diario Oficial de la Federación). 2002. NORMA Oficial Mexicana NOM-021-RECNAT-2000. Que establece las especificaciones de fertilidad, salinidad y clasificación de suelos. Estudios, muestreo y análisis. Gobierno de México. Secretaría del Medio Ambiente y Recursos Naturales. Ciudad de México, México. http://www.ordenjuridico.gob.mx/Documentos/Federal/wo69255.pdf (Retrieved: December 2025).

Han L, Wang C, Meng J, He Y. 2024. Variabilidad espacial de las propiedades físicas y hídricas del suelo en los bosques subtropicales del sur de China. Forests 15 (9): 1590. https://doi.org/10.3390/f15091590

INEGI (Instituto Nacional de Estadística y Geografía). 2017. Anuario estadístico y geográfico de Tabasco 2017. Ciudad de México, México. 443 p.

Li S, Li Q, Wang C, Li B, Gao X, Li Y, Wu D. 2019. Spatial variability of soil bulk density and its controlling factors in an agricultural intensive area of Chengdu Plain, Southwest China. Journal of Integrative Agriculture 18 (2): 290–300. https://doi.org/10.1016/s2095-3119(18)61930-6

Lince-Salazar LA. 2021. Capacidad de almacenamiento de agua en suelos cultivados en café y otras propiedades edáficas relacionadas. Revista Cenicafé 72 (1): e72101. https://doi.org/10.38141/10778/72101

Márquez K. 2021. Caracterización de la textura de suelo en la subcuenca del río Zaratí para la evaluación del sistema de agua subterránea. *In* Congreso Nacional de Ciencia y Tecnología. Asociación Panameña para el Avance de la Ciencia. Ciudad de Panamá, Panamá, pp: 271–277. https://doi.org/10.33412/apanac.2021.3203

Núñez-Ramírez F, Escobosa-García I, Cárdenas-Salazar V, Santillano-Cázares J, Ruelas-Islas J, Preciado-Rangel P, Díaz-Ramírez JB. 2020. Tensión de humedad del suelo, crecimiento, eficiencia en el uso del agua y rendimiento de maíz cultivado en el noroeste de México. Revista Terra Latinoamericana 38 (4): 805–815. https://doi.org/10.28940/terra.v38i4.763

Palma-López DJ, Cisneros-Domínguez J, Moreno-Cáliz E, Rincón-Ramírez A. 2007. Suelos de Tabasco: su uso y manejo sustentable. Colegio de Postgraduados. Fundación Produce Tabasco. Villahermosa, México. 195 p.

Pérez-Zapata J, Delgado BL, Osorio CJ, Bernal MM, Zapata HS. 2024. Variabilidad espacial de propiedades fisicoquímicas en suelos bananeros de Urabá-Colombia. Acorbat Revista de Tecnología y Ciencia 1 (1). https://doi.org/10.62498/artc.2407

Reza S, Nayak D, Chattopadhyay T, Mukhopadhyay S, Singh S, Srinivasan R. 2016. Spatial distribution of soil physical properties of alluvial soils: a geostatistical approach. Archives of Agronomy and Soil Science 62 (7): 972–981. https://doi.org/10.1080/03650340.2015.1107678

Sakaki T, Smits KM. 2015. Water retention characteristics and pore structure of binary mixtures. Vadose Zone Journal 14 (2): 1–7. https://doi.org/10.2136/vzj2014.06.0065

Salamanca-Jiménez A, Lince-Salazar LA, Alzate SNA. 2018. Variabilidad espacial de la densidad aparente del suelo a nivel de lote en café. Revista Cenicafé 69 (2): 47–59.

Sandoval-García C, Cantú-Silva I, González-Rodríguez H, Yánez-Díaz MI, Marmolejo-Monsiváis JG, Gómez-Meza MV. 2021. Efecto de diferentes usos del suelo en las propiedades físicas e hidrológicas de un Luvisol en Oaxaca. Revista Mexicana de Ciencias Forestales 12 (68): 151–177. https://doi.org/10.29298/rmcf.v12i68.982

SEMARNAT (Secretaría de Medio Ambiente y Recursos Naturales). 2024. Mapa con los diferentes grupos de suelos por textura que existen en el territorio mexicano. Gobierno de México. Secretaría de Medio Ambiente y Recursos Naturales. Subsistema de Información sobre el Ordenamiento Ecológico. Ciudad de México, México. https://gisviewer.semarnat.gob.mx/aplicaciones/uga_oe2/ (Retrieved: December 2025).

Suarez-Muñoz BS, Flores-Cadena CA, Cedeño-Bermeo JE, Chóez-Acosta LA. 2025. Modelos matemáticos no lineales aplicados a la agricultura. Revisión sistemática. RECIMUNDO 9 (2): 180–200. https://doi.org/10.26820/recimundo/9.(2).abril.2025.180-200

Varón-Ramírez VM, Araujo-Carrillo GA, Guevara-Santamaría MA. 2022. Colombian soil texture: Building a spatial ensemble model. Earth System Science Data 14 (10): 4719–4741. https://doi.org/10.5194/essd-14-4719-2022

Xu Y, He Q, Lu H, Yang K, Entekhabi D, Gianotti DJ. 2025. A global dataset of remote sensing-based soil critical point and permanent wilting point. Scientific Data 12 (1). https://doi.org/10.1038/s41597-025-05048-y

Yu H, Li X, Zhang Y, Wang J, Chen T. 2025. Spatiotemporal variability of precipitation extremes and their relationship with large-scale climate indices in China. Atmosphere 16 (2): 191. https://doi.org/10.3390/atmos16020191